Compressive inverse scattering using ultrashort pulses

Kyung Hwan Jin[a], Kanghee Lee[b], Jaewook Ahn[b], and Jong Chul Ye[a,*]

[a]Department of Bio and Brain Engineering, KAIST, Daejeon 305-701, Korea;
[b]Department of Physics, KAIST, Daejeon 305-701, Korea

ABSTRACT

Inverse scattering refers the retrieval of the unknown constitutive parameters from measured scattered wave fields, and has many applications such as ultrasound imaging, optics, T-ray imaging, radar, and etc. Two distinct imaging strategies have been commonly used: narrow band inverse scattering approaches using a large number of transmitters and receivers, or wideband imaging approaches with smaller number of transmitters and receivers. In some biomedical imaging applications, the limited accessibility of scattered fields using externally located antenna arrays usually prefers the wideband imaging approaches. The main contribution of this paper is, therefore, to analyze the wideband inverse scattering problem from compressive sensing perspective. Specifically, the mutual coherence of the wideband imaging geometry is analyzed, which reveals a significant advantage to identify the sparse targets from very limited number of measurements.

Keywords: pulsed terahertz imaging, compressed sensing, reflectance tomography, inverse scattering, coherent imaging

1. INTRODUCTION

One of the fundamental questions in wave scattering theory is to retrieve unknown constitutive properties from measured scattering fields. Such problem - often called inverse scattering - has numerous applications in practice, such as ultrasound imaging,[1] microwave imaging,[2] terahertz imaging,[3] radar, geophysical applications,[4] and etc. Especially important form of the inverse scattering problem arises from scalar Helmholtz wave equation. For example, in electromagnetic wave propagation, if the polarization effects of the wave can be negligible, the vector Maxwell equation can be approximated using a scalar wave equation.[3] In ultrasound imaging, the sound propagation can be modeled as a scalar wave.

Two types of acquisition scheme have been currently used: narrow band imaging and wideband imaging techniques using pulse or ultrawide band signals.[4] The narrow band techniques generally require a large number of source and detector pairs to be distributed around the object of interest. In contrast, wideband imaging approaches seek to identify the presence and location of significant scatterers in the medium from reflected fields. In many medical applications of inverse scattering, the wideband imaging is more appropriate due to the limited accessibility of the scattered measurements.

Recently, compressed sensing has become the main stream of research in signal processing community. More specifically, if the unknown signal is sparse and the sensing dictionary is sufficiently incoherent from the modeling dictionary, compressive sensing tells us that perfect reconstruction is possible from very limited number of samples under Nyquist limit.[5] Considering the significant impact of the compressive sensing in many imaging area,[6–9] we are interested in analyzing the performance limit of this inverse scattering problem. Narrow band inverse scattering approach has been recently analyzed from compressive sensing perspective,[10,11] which demonstrates that sparse objects can be reconstructed significantly well using smaller number of antenna arrays. However, we are not aware of any results for the wide-band imaging problem. Therefore, the main goal of this paper is to extend the analysis for wideband imaging problem.

Further author information: (Send correspondence to Jong Chul Ye)
Jong Chul Ye: E-mail: jong.ye@kaist.ac.kr, Telephone: 82-42-350-4320

Computational Imaging VIII, edited by Charles A. Bouman, Ilya Pollak, Patrick J. Wolfe,
Proc. of SPIE-IS&T Electronic Imaging, SPIE Vol. 7533, 75330D · © 2010 SPIE-IS&T
CCC code: 0277-786X/10/$18 · doi: 10.1117/12.849068

The main application of our theory is terahertz imaging (T-ray imaging). The terahertz pulse has broad spectrum ranges of $0.1 \sim 10$THz. A standard method to measure the terahertz pulse shape is based on the correlation with the reference pulse, which is known as terahertz time domain spectroscopy (THz-TDS). In classical terahertz imaging techniques, the THz beam is brought to an intermediate focus, and imaging targets are inserted into the region where the THz beam is collimated. This requires a time consuming point-by-point raster scanning.[12] Based on the inverse scattering theory for ultra-wideband signal, we develop a compressive acquisition scheme for THz imaging. Then, the compressive sensing theory provides an opportunity to reduce acquisition time by reducing the number of pulse measurements.

2. THEORY

2.1 Volume Scattering

Assume that the scalar field ψ follows the Helmholtz equation:

$$\nabla^2\psi(\mathbf{r},k) + k^2 n^2(\mathbf{r})\psi(\mathbf{r},k) = -S(\mathbf{r},k) \ , \tag{1}$$

where $S(\mathbf{r},k)$ denotes the source spectrum at $\mathbf{r} = (x,y,z)$, $k = 2\pi/\lambda$ is the wave number, and $n(\mathbf{r})$ is the refractive index, respectively. This can be equivalently represented as

$$\nabla^2\psi(\mathbf{r},k) + k^2\psi(\mathbf{r},k) = -S(k;\mathbf{r}) - k^2 F(\mathbf{r})\psi(\mathbf{r},k) \tag{2}$$

with unknown reflectivity variations $F(\mathbf{r}) = n^2(\mathbf{r}) - 1$, in case the refractive index of inhomogeneous materials is almost independent to wavelength. The homogeneous Green's function satisfies

$$\left(\bigtriangledown^2 + k^2\right) g_k(\mathbf{r}|\mathbf{r}) = -\delta(\mathbf{r}-\mathbf{r}') \ , \tag{3}$$

whose fundamental solution under free space boundary condition is given by

$$g_k(\mathbf{r}|\mathbf{r}') = \frac{e^{ik|\mathbf{r}-\mathbf{r}'|}}{4\pi|\mathbf{r}-\mathbf{r}'|}. \tag{4}$$

Similarly, the homogeneous incident field is given by

$$\nabla^2\psi_i(\mathbf{r},k) + k^2\psi_i(\mathbf{r},k) = -S(\mathbf{r},k). \tag{5}$$

Then, under the Born approximation that asserts $\psi(\mathbf{r}',k) \simeq \psi_i(\mathbf{r}',k)$, the scattered field $\psi_s(\mathbf{r},k) = \psi(\mathbf{r},k) - \psi_i(\mathbf{r},k)$ can be represented as

$$\psi_s(\mathbf{r};k) \simeq k^2 \int d\mathbf{r}' F(\mathbf{r}') g_k(\mathbf{r}|\mathbf{r}')\psi_i(\mathbf{r}';k) \ . \tag{6}$$

Suppose an isotropic point source with power spectrum $S(k)$ is located at $\mathbf{r}_t$, and the scattered field are measured at $\mathbf{r}$ as shown in Fig. 1(a). In this case, the incident field $\psi_i(\mathbf{r}',k)$ is given by

$$\psi_i(\mathbf{r}',k) = S(k) g_k(\mathbf{r}_t|\mathbf{r}') \ . \tag{7}$$

Hence, the final form of the scattering measurement is given by

$$y(\mathbf{r};k) \triangleq \frac{\psi_s(\mathbf{r};k)}{k^2 S(k)} \simeq \int d\mathbf{r}' F(\mathbf{r}') g_k(\mathbf{r}|\mathbf{r}') g_k(\mathbf{r}_t|\mathbf{r}') \ . \tag{8}$$

Now, let $y(\mathbf{r};\bar{t}) = \int y(\mathbf{r};k) e^{-jk\bar{t}} dk$ denote the inverse Fourier transform, $\bar{t}$ denotes the normalized time with respect to the speed of light such that $\bar{t} = ct$, and $\delta(\cdot)$ denotes the Kronecker delta function. Then, Eq. (8) can be represented in time domain as following:

$$y(\mathbf{r};\bar{t}) \quad = \quad \int d\mathbf{r}' F(\mathbf{r}') \frac{\delta\left(\bar{t} - |\mathbf{r}'-\mathbf{r}| - |\mathbf{r}'-\mathbf{r}_t|\right)}{(4\pi)^2 |\mathbf{r}'-\mathbf{r}||\mathbf{r}'-\mathbf{r}_t|}. \tag{9}$$

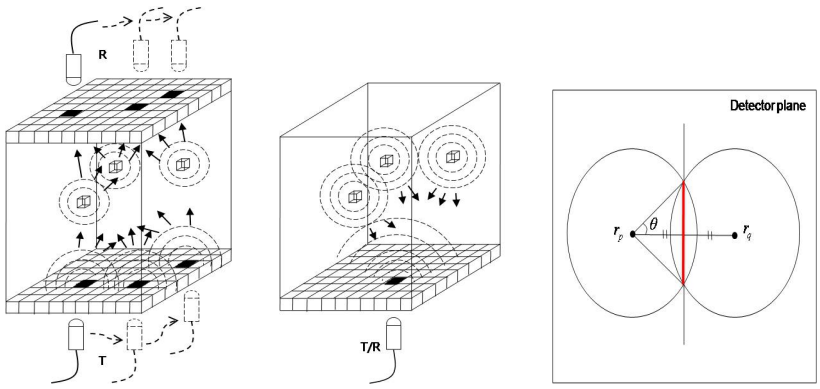

(a) (b) (c)

Figure 1: Geometry of (a) transmission mode THz tomography, (b) pulse-echo mode THz tomography with co-location transmit/reciever, and (c) a top view of equi-radius map from distinct voxels. The red line($\mathbf{r}_r$) corresponds to the equidistance line from $\mathbf{r}_p$ and $\mathbf{r}_q$. T: transmitter R: receiver

In practice, the source spectrum is bandlimited, i.e. $S(k) = S(k)\Pi_{k_0}(k)$, where k_0 denotes the bandwidth and $\Pi_{k_0}(k)$ is an indicator function of the spectrum interval $[-k_0, k_0]$. Then, Eq. (9) can be modified as

$$\begin{aligned} y(\mathbf{r};\bar{t}) &= b(\bar{t}) * \int d\mathbf{r}' F(\mathbf{r}') \frac{\delta\left(\bar{t} - |\mathbf{r}' - \mathbf{r}| - |\mathbf{r}' - \mathbf{r}_t|\right)}{(4\pi)^2 |\mathbf{r}' - \mathbf{r}||\mathbf{r}' - \mathbf{r}_t|} \\ &= \int d\mathbf{r}' F(\mathbf{r}') \frac{b\left(\bar{t} - |\mathbf{r}' - \mathbf{r}| - |\mathbf{r}' - \mathbf{r}_t|\right)}{(4\pi)^2 |\mathbf{r}' - \mathbf{r}||\mathbf{r}' - \mathbf{r}_t|} , \end{aligned} \tag{10}$$

where $b(t) = \sin(k_0 t)/(\pi t)$. For monostatic case as shown in Fig. 1(b), i.e. $\mathbf{r} = \mathbf{r}_t$, Eq. (10) can be further simplified as

$$y(\mathbf{r};\bar{t}) = \int d\mathbf{r}' F(\mathbf{r}';\bar{t}) \frac{b\left(\bar{t} - 2|\mathbf{r} - \mathbf{r}'|\right)}{(4\pi)^2 |\mathbf{r} - \mathbf{r}'|^2}. \tag{11}$$

2.2 Scattering From Planar Aperture

Wave scattering measurement from a planar aperture can be analyzed using Hyugens-Fresnel principle.[13] Let $\boldsymbol{\rho} = (x, y)$ denotes a lateral coordinate. Under Fresnel approximation, the resulting expression for the scattering field at $\mathbf{r} = (\boldsymbol{\rho}, z)$ from a planar aperture with transmittance $F(\boldsymbol{\rho}')$ located at z' is given by

$$\psi_s(\boldsymbol{\rho}, z; k) = \int d\boldsymbol{\rho}' F(\boldsymbol{\rho}') g_k(\boldsymbol{\rho}, z; \boldsymbol{\rho}', z') \tag{12}$$

where the Green's function from Fresnel approximation is given by

$$g_k(\boldsymbol{\rho}, z; \boldsymbol{\rho}', z') = \frac{k e^{ik|z - z'|}}{i2\pi|z - z'|} \exp\left(\frac{ik}{2|z - z'|}|\boldsymbol{\rho} - \boldsymbol{\rho}'|^2\right). \tag{13}$$

Suppose the incident field is a planar wave whose propagation direction is along the positive z-direction, i.e. $\psi_i(\boldsymbol{\rho}', z') = e^{ikz}$. Then, the scattering field measurement from the planar aperture at $z' = 0$ is given by a 2-D convolution:

$$\begin{aligned} \psi_s(\boldsymbol{\rho}, z; k) &= F(\boldsymbol{\rho}) * h(\boldsymbol{\rho}) \\ &= \frac{k e^{ikz}}{i2\pi z} e^{i\frac{k}{2z}|\boldsymbol{\rho}|^2} \int d\boldsymbol{\rho}' \left\{ F(\boldsymbol{\rho}') e^{i\frac{k}{2z}|\boldsymbol{\rho}'|^2} \right\} e^{-i\frac{k}{z}\boldsymbol{\rho}^T \boldsymbol{\rho}'} \end{aligned} \tag{14}$$

where the convolution kernel $h(\boldsymbol{\rho})$ and its Fourier transform are given by

$$h(\boldsymbol{\rho}) = \frac{k e^{ikz}}{i2\pi z} e^{\frac{ik}{2z}|\boldsymbol{\rho}|^2} \quad , \quad \tilde{H}(\mathbf{q}) = e^{ikz} e^{-i\frac{z|\mathbf{q}|^2}{2k}} . \tag{15}$$

In the diffraction imaging applications as shown in Fig. 2, the measurement is directly taken from the scattering measurement without using lens. In this case, by defining $y(\mathbf{r};k) \triangleq \frac{\psi_s(\mathbf{r};k)}{\left(\frac{ke^{ikz}}{i2\pi z}\right)}$ and taking the inverse Fourier transform along k, we have

$$y(\mathbf{r};\bar{t}) = \int d\boldsymbol{\rho}' F(\boldsymbol{\rho}')\delta\left(\bar{t} - \frac{|\boldsymbol{\rho}-\boldsymbol{\rho}'|^2}{2z}\right) \tag{16}$$

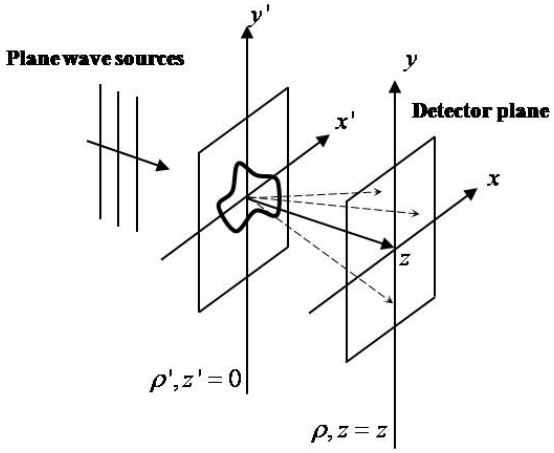

Figure 2: Diffraction imaging acquisition setup for Eq.(16)

Another interesting system is an image domain acquisition system with 4-f setup as illustrated in Fig. 3(a). Only difference from the conventional 4-f system is the existence of an offcentered pinhole aperture on the Fourier plane. According to Fourier optics,[13] a thin lens with focal length f corresponds the phase transformer of the following form:

$$t_l(\boldsymbol{\rho}) = e^{-i\frac{k}{2f}|\boldsymbol{\rho}|^2} \ . \tag{17}$$

Hence, for the geometry in Fig. 3(a), the field at $z = 2f$ is given by

$$\begin{aligned} U_2(\boldsymbol{\rho}) &= \{U_1(\boldsymbol{\rho})t_l(\boldsymbol{\rho})\} * h(\boldsymbol{\rho}) \\ &= \frac{ke^{ikf}}{i2\pi f} e^{i\frac{k}{2f}|\boldsymbol{\rho}|^2} \int d\boldsymbol{\rho}' U_1(\boldsymbol{\rho}') e^{-i\frac{k}{f}\boldsymbol{\rho}^T\boldsymbol{\rho}'} \\ &= \frac{ke^{ikf}}{i2\pi f} e^{i\frac{k}{2f}|\boldsymbol{\rho}|^2} \tilde{U}_1\left(\frac{k}{f}\boldsymbol{\rho}\right) \\ &= \frac{ke^{ikf}}{i2\pi f} e^{i\frac{k}{2f}|\boldsymbol{\rho}|^2} \tilde{F}\left(\frac{k}{f}\boldsymbol{\rho}\right)\tilde{H}\left(\frac{k}{f}\boldsymbol{\rho}\right) \\ &= \frac{ke^{ik2f}}{i2\pi f}\tilde{F}\left(\frac{k}{f}\boldsymbol{\rho}\right) \ , \end{aligned} \tag{18}$$

where $U_1(\boldsymbol{\rho}) = \psi_s(\boldsymbol{\rho}, f; k)$ and $\tilde{U}_1, \tilde{F}$ and $\tilde{H}$ denote the Fourier transform of U_1, F and H, respectively. Similarly, the field at $4f$ is given by

$$U_4(\boldsymbol{\rho}) = \frac{ke^{ik2f}}{i2\pi f}\tilde{U}_2\left(\frac{k}{f}\boldsymbol{\rho}\right) \ . \tag{19}$$

Therefore, if a point detector is located at the optical axis, the detector reading from the scattering field through a circular pinhole at the Fourier plane as shown in Fig. 3(b) is given by

$$U_4(\mathbf{0}) = \frac{ke^{ik2f}}{i2\pi f}\tilde{U}_2(\mathbf{0}) = \left(\frac{ke^{ik2f}}{i2\pi f}\right)^2 \int_{|\boldsymbol{\rho}'-r\mathbf{s}_\theta|\le\frac{a}{2}} \tilde{F}\left(\frac{k}{f}\boldsymbol{\rho}'\right) d\boldsymbol{\rho}' \tag{20}$$

where $\mathbf{s}_\theta = (\cos\theta, \sin\theta)$. This can be further simplified as

$$\begin{aligned} U_4(\mathbf{0}) &= \left(\frac{ke^{ik2f}}{i2\pi f}\right)^2 \int \tilde{F}\left(\frac{k}{f}x', \frac{k}{f}y'\right) \mathrm{circ}_a(r\cos\theta - x', r\sin\theta - y')dx'dy' \\ &= \left(\frac{ke^{ik2f}}{i2\pi f}\right)^2 \int d\boldsymbol{\rho} F(\boldsymbol{\rho}) a^2 \mathrm{jinc}\left(\frac{ak}{2\pi f}|\boldsymbol{\rho}|\right) e^{-ik\frac{r}{f}\boldsymbol{\rho}^T \mathbf{s}_\theta} , \end{aligned} \tag{21}$$

where $\mathrm{circ}_a(x,y)$ and $\mathrm{jinc}(t)$ are defined as

$$\mathrm{circ}_a(x,y) = \begin{cases} 1 & \sqrt{x^2+y^2} \le \frac{a}{2}; \\ 0 & \text{otherwise.} \end{cases} , \tag{22}$$

$$\mathrm{jinc}(t) = \frac{J_1(\pi t)}{2t} \tag{23}$$

and $J_1(t)$ is the first order Bessel function of the first kind. If $a \to 0$, $\mathrm{jinc}\left(\frac{ak}{2\pi f}|\boldsymbol{\rho}|\right)$ approach a flat function with value of $\pi/4$. Hence, by defining $y(\theta;k) \triangleq \frac{U_4(0)}{\left(\frac{ke^{ik2f}}{i2\pi f}\right)^2}$ and taking the inverse Fourier transform along k, we have the following approximation:

$$\begin{aligned} y(\theta;\bar{t}) &\approx \frac{a^2\pi}{4} \int d\boldsymbol{\rho}' F(\boldsymbol{\rho}') \delta\left(\bar{t} - \frac{r}{f}\mathbf{s}_\theta^T \boldsymbol{\rho}'\right) \\ &= \frac{fa^2\pi}{4r} \int d\boldsymbol{\rho}' F(\boldsymbol{\rho}') \delta\left(\mathbf{s}_\theta^T \boldsymbol{\rho}' - \frac{f}{r}\bar{t}\right) \end{aligned} \tag{24}$$

which corresponds to the Radon transform of $F(\boldsymbol{\rho})$.

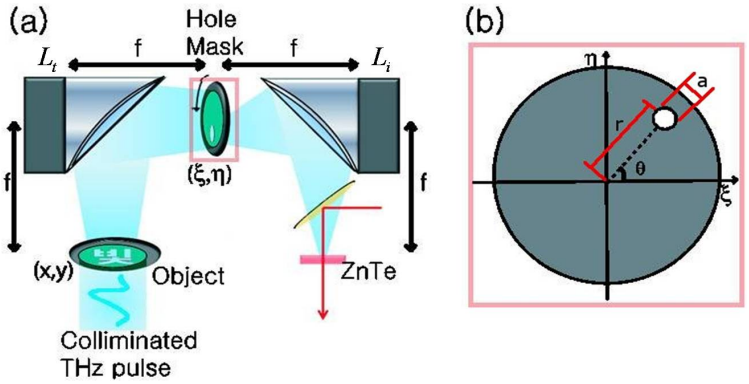

Figure 3: (a) An experimental setup of proposed planar aperture imaging. (b) A geometry of an off-centered aperture.

3. INVERSE PROBLEM

3.1 Volume Scattering

Let $\{\mathbf{r}_n\}_{n=1}^N$ denote the transmit/receiver antenna positions for a monostatic acquisition, and $\{\mathbf{r}'_p\}_{p=1}^P$ gives the voxel positions within the field of view(FOV), respectively; $\{\bar{t}_l\}_{l=1}^L$ is the sampling time of the THz waveform. Note that $\bar{t}_L$ denotes the maximum travel distance from a transmitter to a target to a receive antenna; hence, it determines the FOV. Then, Eq. (9) can be represented as the following matrix equation:

$$\mathbf{y}^{(n)} = \mathbf{G}^{(n)}\mathbf{f} , \quad n = 1, \ldots, N , \tag{25}$$

where $\mathbf{y}^{(n)} = [y(\mathbf{r}_n;\bar{t}_1),\cdots,(\mathbf{r}_n;\bar{t}_L)]^T$, $\mathbf{f} = V/(4\pi)^2\,[F(\mathbf{r}'_1),\cdots,F(\mathbf{r}'_P)]^T$, and V denotes the voxel volume, respectively; and $\mathbf{G}^{(n)}$ is given by

$$\begin{bmatrix} \frac{\delta(\bar{t}_1-2|\mathbf{r}_n-\mathbf{r}'_1|)}{|\mathbf{r}_n-\mathbf{r}'_1|^2} & \cdots & \frac{\delta(\bar{t}_1-2|\mathbf{r}_n-\mathbf{r}'_P|)}{|\mathbf{r}_n-\mathbf{r}'_1|^2} \\ \vdots & \ddots & \vdots \\ \frac{\delta(\bar{t}_L-2|\mathbf{r}_n-\mathbf{r}'_1|)}{|\mathbf{r}_n-\mathbf{r}'_1|^2} & \cdots & \frac{\delta(\bar{t}_L-2|\mathbf{r}_n-\mathbf{r}'_P|)}{|\mathbf{r}_n-\mathbf{r}'_1|^2} \end{bmatrix} , \tag{26}$$

which usually has very sparse non-zero elements.0 Stacking together the measurement vector at every transmit/receive antenna position, we have

$$\mathfrak{y} = \mathfrak{G}\ \mathbf{f} + \mathbf{n}\ , \tag{27}$$

where $\mathfrak{y} = [\mathbf{y}^{(1)T},\cdots,\mathbf{y}^{(N)T}]^T \in \mathbb{R}^{NL\times 1}$, $\mathfrak{G} = [\mathbf{G}^{(1)T},\cdots,\mathbf{G}^{(N)T}]^T \in \Re^{NL\times P}$ and $\mathbf{n}$ is the noise from system, respectively. Under the assumption that the support of the targets is sparse, the sparse recovery problem can then be reformulated as:

$$(P0): \quad \min\ ||\mathbf{f}||_0, \quad \text{subject to } \|\mathfrak{y}-\mathfrak{G}\ \mathbf{f}\|_2 \le \epsilon, \tag{28}$$

where $||\mathbf{f}||_0$ denotes the number of non-zero elements of $\mathbf{f}$. However, (P0) is a combinatorial optimization problem; thus, convex relaxation using l_1 minimization or a greedy method has been extensively investigated, which states that a bound for the maximum number of recoverable targets is given by

$$||\mathbf{f}||_0 \quad < \quad \left(\mu(\mathfrak{G})^{-1}+1\right)/2\ , \tag{29}$$

where $\mu(\mathfrak{G})$ denotes the so called *mutual coherence*.[14] Note that smaller mutual coherence implies that significant acceleration is possible during acquisition. Assuming sufficiently small voxel size, we can easily show that the mutual coherence $\mu(\mathfrak{G})$ can be represented as

$$\max_{p\neq q} \frac{\sum_{n\in\mathcal{N}_{pq}} \frac{1}{|\mathbf{r}_n-\mathbf{r}'_p|^2|\mathbf{r}^s_n-\mathbf{r}'_q|^2}}{\left(\sum_{n=1}^N \frac{1}{|\mathbf{r}_n-\mathbf{r}'_p|^2}\right)^{\frac{1}{2}}\left(\sum_{n=1}^N \frac{1}{|\mathbf{r}_n-\mathbf{r}'_q|^2}\right)^{\frac{1}{2}}}\ , \tag{30}$$

where the index set $\mathcal{N}_{pq}$ is given by

$$\mathcal{N}_{pq} = \left\{n\in\{1,\cdots,N\} : \left|\mathbf{r}'_p-\mathbf{r}_n\right| = \left|\mathbf{r}'_q-\mathbf{r}_n\right|\right\}\ . \tag{31}$$

Note that the index $\mathcal{N}_{pq}$ denotes the transmit/receive antenna indices whose center position is located at an equi-distance plane perpendicular to the connecting line between $\mathbf{r}'_p$ and $\mathbf{r}'_q$, as illustrated in Fig. 1(c). Therefore, if we choose the transmit/receive antenna scan positions such that no more than two center positions are collinear, the cardinality of the set $\mathcal{N}$ is 2. In particular, for the far field targets, this implies that $\mu(\mathfrak{G}) \simeq 2/N \ll 1$, since the distances from the transmit or receive antenna to each voxel are approximately the same. This implies that the worst case bound of sparse recovery is $\frac{N}{4}$, which is the same order of number of measurements.

3.2 Scattering from Planar Aperture

We can consider the case of planar aperture imaging system in a similar way to the case of volume scattering. We convert analytic forms of optical system to sequence forms. Eq.(24) can be represented in the matrix equation:

$$\mathbf{y}(\theta_n) = \mathbf{a}(\theta_n)\mathbf{f}, \quad n = 1,\ldots,N \tag{32}$$

where $\mathbf{f} = \frac{fa^2\pi}{4r}[F(\boldsymbol{\rho}_1),\ldots,F(\boldsymbol{\rho}_P)]^T$, $\mathbf{y}(\theta_n) = [y(\theta_n,\bar{t}_1),\ldots,y(\theta_n,\bar{t}_L)]^T$ is the columnwise vectorization of 2D matrix, and L is the number of time domain samples; and $\mathbf{a}(\theta_n)$ is given by

$$\begin{bmatrix} \delta\left(x_1\cos(\theta_n)+y_1\cos(\theta_n)-\frac{f}{r}\bar{t}_1\right) & \cdots & \delta\left(x_P\cos(\theta_n)+y_P\cos(\theta_n)-\frac{f}{r}\bar{t}_1\right) \\ \vdots & \ddots & \vdots \\ \delta\left(x_1\cos(\theta_n)+y_1\cos(\theta_n)-\frac{f}{r}\bar{t}_L\right) & \cdots & \delta\left(x_P\cos(\theta_n)+y_P\cos(\theta_n)-\frac{f}{r}\bar{t}_L\right) \end{bmatrix} . \tag{33}$$

These partial matrices can be stacked by the column direction,

$$\mathbf{Y} = \mathbf{A}\mathbf{f} + \mathbf{n} \tag{34}$$

where $\mathbf{S} = [\mathbf{s}(\theta_1)^T, \cdots, \mathbf{s}(\theta_N)^T]^T \in \mathbb{R}^{NL\times 1}$, $\mathbf{A} = [\mathbf{a}(\theta_1)^T, \cdots, \mathbf{a}(\theta_N)^T]^T \in \mathbb{R}^{NL\times P}$ and $\mathbf{n}$ is the noise from system, respectively. The mutual coherence $\mu(A)$ of sensing dictionary A between distinct two points is derived as

$$\max_{p\neq q} \frac{\sum_{n\in\mathcal{N}_{pq}} 1}{(\sum_{n=1}^{N} 1)^{1/2}(\sum_{n=1}^{N} 1)^{1/2}}, \tag{35}$$

where the index set $\mathcal{N}_{pq}$ is given by

$$\mathcal{N}_{pq} = \{n \in \{1, \cdots, N\} : x_q \cos(\theta_n) + y_q \sin(\theta_n) = x_p \cos(\theta_n) + y_p \sin(\theta_n)\} \ . \tag{36}$$

The cardinality of the set $\mathcal{N}$ is 1. This is because if the acquisition angles are restricted to $[0, \pi]$, there exists only one projection angle such that a parallel ray passes two distinct points.

4. NUMERICAL RESULTS AND EXPERIMENTAL RESULTS

We performed a simulation for the pulse-echo mode reflection tomography. In order to verify our analysis for mutual coherence, two detector configurations were considered. In this simulation, the size of phantom is $17 \times 17 \times 17$ and the number of non-zero voxels in the phantom is 72. The pitch of voxel is $5mm$ and the number of detector is 33. The signal to noise ratio is 6dB. In Fig. 4(b), detectors are co-linearly located, which provides inaccurate reconstruction using orthogonal matching pursuit(OMP).[14] In Fig. 4(c), the position of detectors are randomly distributed. Even though same number of detectors are used, the OMP algorithm provides very accurate reconstruction. In the simulation, the source has a broad spectrum ranges from 0 to 2THz. The comparison between Fig. 4(b) and Fig. 4(c) reveals the advantage of optimizing mutual coherence.

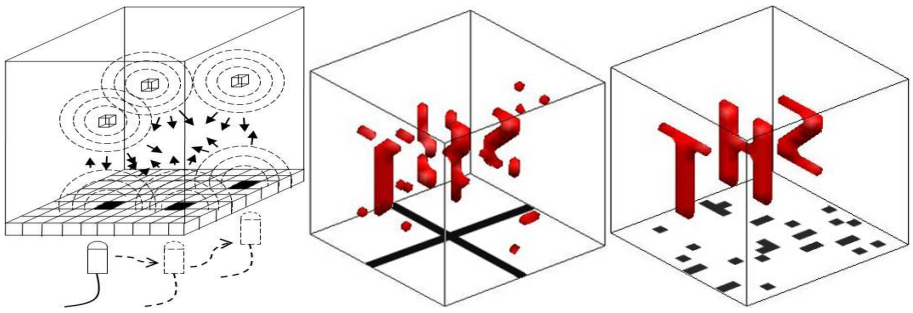

(a) (b) (c)

Figure 4: (a) Pulse echo mode configuration. Reconstruction results using (b) co-linearly positioned detectors, and (c) randomly positioned detectors.

Next, we performed a real experiment for the planar aperture acquisition system as illustrated in Fig. 3(a). For the experiment, we used a Ti:sapphire laser oscillator which produced 50-fs-short pulses at a repetition rate of 100 MHz. The average power and the wavelength of the laser were 350 mW and ∼800 nm, respectively. For the generation and detection of THz waves, a large-area photoconductive antenna (PCA)[15] and a 1-mm-thick ZnTe electro-optic crystal were used. The offcentered aperture was fabricated with a 5-mm-diameter hole which was 15 mm off from the optic axis. A first parabolic mirror with $f = 150$ mm was used as the transform optic L_t. The second parabolic mirror used as the imaging optic L_i had a short focal length of $f' = 100$ mm for a tight focus of the diffracted THz waves onto the detector, which was located at the center of the image plane. The time-domain signal of the THz wave was collected to retrieve the THz spectrum of up to 1.5 THz with a resolution of ∼0.01 THz. We acquired 30 waveforms at every 6 degree. The 2-D aperture in Fig. 5(a) was fabricated using metal plate, and has holes that represent 'light' in Korean. The reconstruction result using inverse radon transform in Fig. 5(b) results in radial aliasing artifacts. The l_1 minimization approach provides clearer image as shown in Fig. 5(c).

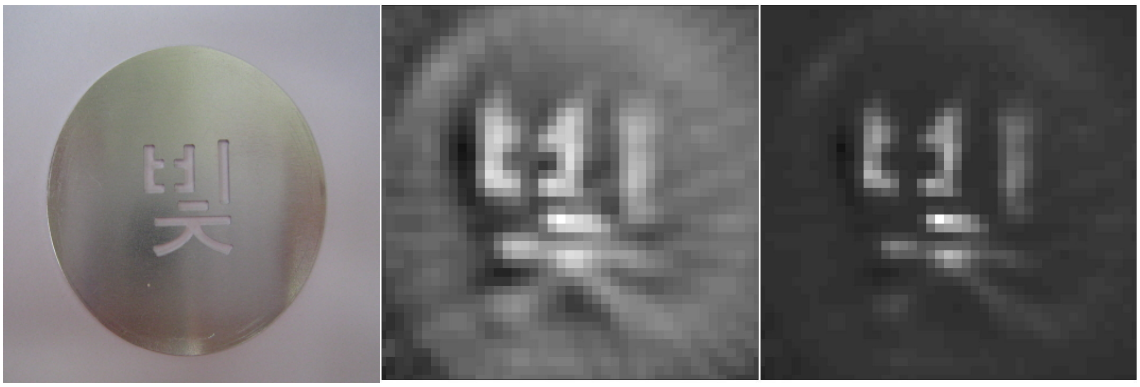

(a) (b) (c)

Figure 5: (a) An optical image of the target aperture. Reconstruction using (b) inverse radon transform, and (c) l_1 minimization algorithm.

5. SUMMARY

We established ultrawide-band inverse scattering theory. We considered the several geometries of ultrawide-band illumination, such as volume scattering and scattering of planar aperture. In the geometry of volume scattering and scattering from planar aperture, the diffraction integral is expressed in terms of the matrix. The mutual coherence of such a matrix is small in time domain. Because the mutual coherence is inversely proportional to the maximum number of recoverable targets in compressed sensing, the reconstruction algorithm based on the compressed sensing theory is appropriate for the ultrawide-band inverse scattering problem. The simulations and experimental results verify our theory.

ACKNOWLEDGMENTS

This work is supported by Korea Science and Engineering Foundation (2009-0081089).

REFERENCES

[1] S. Norton and M. Linzer, "Ultrasonic reflectivity imaging in three dimensions: Exact inverse scattering solutions for plane, cylindrical, and spherical apertures," *IEEE Trans. Biomedical Engineering* **BME-28**, pp. 202–220, February 1981.

[2] E. Bond, X. Li, S. Hagness, and B. Van Veen, "Microwave imaging via space-time beamforming for early detection of breast cancer," *IEEE Transactions on Antennas and Propagation* **51**(8), pp. 1690–1705, 2003.

[3] S. Wang and X.-C. Zhang, "Pulsed terahertz tomography," *Journal of Physics D: Applied Physics* **37**(4), pp. R1–R36, 2004.

[4] A. Kak and M. Slaney, "Principles of computerized tomographic imaging," *New York* , 1999.

[5] D. L. Donoho, "Compressed sensing," *IEEE Trans. on Information Theory* **52**, pp. 1289–1306, April 2006.

[6] M. Lustig, D. Donoho, and J. Pauly, "Sparse MRI: The application of compressed sensing for rapid MR imaging," *Magnetic Resonance in Medicine* **58**(6), pp. 1182–1195, 2007.

[7] H. Jung, K. Sung, K. Nayak, E. Kim, and J. Ye, "kt FOCUSS: a general compressed sensing framework for high resolution dynamic MRI," *Magnetic Resonance in Medicine* **61**(1), 2009.

[8] G. Chen, J. Tang, and S. Leng, "Prior image constrained compressed sensing (PICCS): a method to accurately reconstruct dynamic CT images from highly undersampled projection data sets," *Medical physics* **35**, p. 660, 2008.

[9] E. Sidky and X. Pan, "Image reconstruction by constrained, total-variation minimization," *Physics in medicine and biology* **53**, pp. 4777–4807, 2008.

[10] A. Fannjiang, "Compressive inverse scattering I. High frequency SIMO measurements," *arXiv* **906**.

[11] A. Fannjiang, "Compressive inverse scattering II. SISO measurements with Born scatterers," *Arxiv preprint arXiv:0908.4072* , 2009.
[12] B. Hu and M. Nuss, "Imaging with terahertz waves," *Opt. Letters* **20**(16), p. 1716, 1995.
[13] J. Goodman, *Introduction to Fourier optics*, Roberts & Company Publishers, 2005.
[14] J. Tropp, "Greed is good: algorithmic results for sparse approximation," *IEEE Trans. on Information Theory* **50**(10), pp. 2231–2242, 2004.
[15] A. Dreyhaupt, S. Winnerl, T. Dekorsy, and M. Helm, "High-intensity terahertz radiation from a microstructured large-area photoconductor," *Applied Physics Letters* **86**, p. 121114, 2005.